ACS Catalysis

Research Article

pubs.acs.org/acscatalysis

Hydride Transfer versus Deprotonation Kinetics in the Isobutane–Propene Alkylation Reaction: A Computational Study

Chong Liu,[†,⊥] Rutger A. van Santen,[*,†,‡] Ali Poursaeidesfahani,[§] Thijs J. H. Vlugt,[§] Evgeny A. Pidko,[*,†,‡,∥,⊥] and Emiel J. M. Hensen[†]

[†]Inorganic Materials Chemistry Group, Schuit Institute of Catalysis, and [‡]Institute for Complex Molecular Systems, Eindhoven University of Technology, P.O. Box 513, 5600 MB Eindhoven, The Netherlands

[§]Process & Energy Department, Delft University of Technology, Leeghwaterstraat 39, 2628CB Delft, The Netherlands

[∥]TheoMAT group, International Laboratory "Solution Chemistry of Advanced Materials and Technologies", ITMO University, Lomonosova 9, St. Petersburg 191002, Russia

Supporting Information

ABSTRACT: The alkylation of isobutane with light alkenes plays an essential role in modern petrochemical processes for the production of high-octane gasoline. In this study we have employed periodic DFT calculations combined with microkinetic simulations to investigate the complex reaction mechanism of isobutane–propene alkylation catalyzed by zeolitic solid acids. Particular emphasis was given to addressing the selectivity of the alkylate formation versus alkene formation, which requires a high rate of hydride transfer in comparison to the competitive oligomerization and deprotonation reactions resulting in catalyst deactivation. Our calculations reveal that hydride transfer from isobutane to a carbenium ion occurs via a concerted C–C bond formation between a *tert*-butyl fragment and an additional olefin, or via deprotonation of the *tert*-butyl fragment to generate isobutene. A combination of high isobutane concentration and low propene concentration at the reaction center favor the selective alkylation. The key reaction step that has to be suppressed to increase the catalyst lifetime is the deprotonation of carbenium intermediates that are part of the hydride transfer reaction cycle.

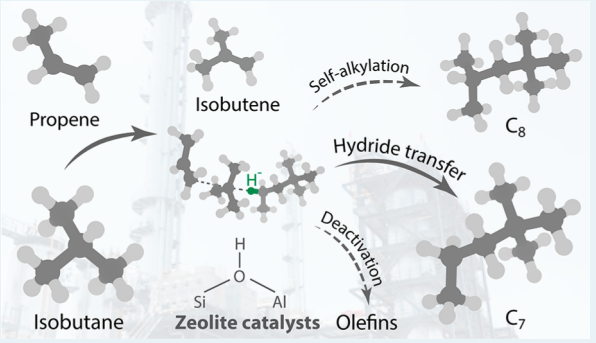

KEYWORDS: *hydride transfer, alkylation, deactivation, faujasite, periodic DFT, microkinetics*

1. INTRODUCTION

Catalysis by solid acids is a powerful tool for the conversion of relatively unreactive molecules such as alkanes or methanol into a wide range of useful products.[1] In most cases, the practical applicability of these systems is limited by the fast catalyst deactivation that is commonly addressed by combining the catalytic reaction system with catalyst regeneration systems, which increases the complexity of the overall process and introduces severe constraints on the potential catalyst materials.[2]

Acid-catalyzed alkylation of isobutane with light alkenes is one of the cornerstone technologies to produce high-octane gasoline in petroleum refineries.[3,4] The main challenge to the alkylation chemistry is to develop a solid acid catalyst for this process, which can compete with current highly optimized technologies based on liquid mineral acids such as HF and H_2SO_4. A wide range of solid acids has been investigated, including supported Brønsted and Lewis acids, exchange resins, zeolites, sulfated transition-metal oxides, and heteropolyacids and their derivatives.[5,6] Ionic liquids, although not true solid acids, have also been explored for the development of greener alkylation processes.[7] Zeolite-type solid acids have been in the spotlight of academic and industrial research as the most promising catalysts for heterogeneous alkylation. The common fundamental challenge of solid acid catalyzed reactions is catalyst stability, which in most processes requires periodic catalyst rejuvenation and reactivation steps. A main cause of such deactivation reactions is the oligomerization of alkene intermediates, implying that their formation should be suppressed for efficient catalysis.[8] For the catalytic cracking process, the hydride transfer processes were found to be essential to suppress such reactions.[9,10] Hydride transfer reactions in the methanol to hydrocarbon (MTH) process largely control the steady-state concentration of alkenes and arenes in zeolite pores and therefore the relationship between the catalytic alkene and arene cycles (dual-cycle mechanism), which affects the final MTH product distribution.[11] Recently, Lercher et al.[12] have identified that such hydride transfer reactions involve both Lewis and Brønsted acid sites. The competition between the hydride transfer and alkene formation

Received: August 25, 2017
Revised: November 1, 2017
Published: November 9, 2017

DOI: 10.1021/acscatal.7b02877
ACS Catal. 2017, 7, 8613–8627

Scheme 1. Reaction Network of the Catalytic Isobutane−Propene Alkylation[a]

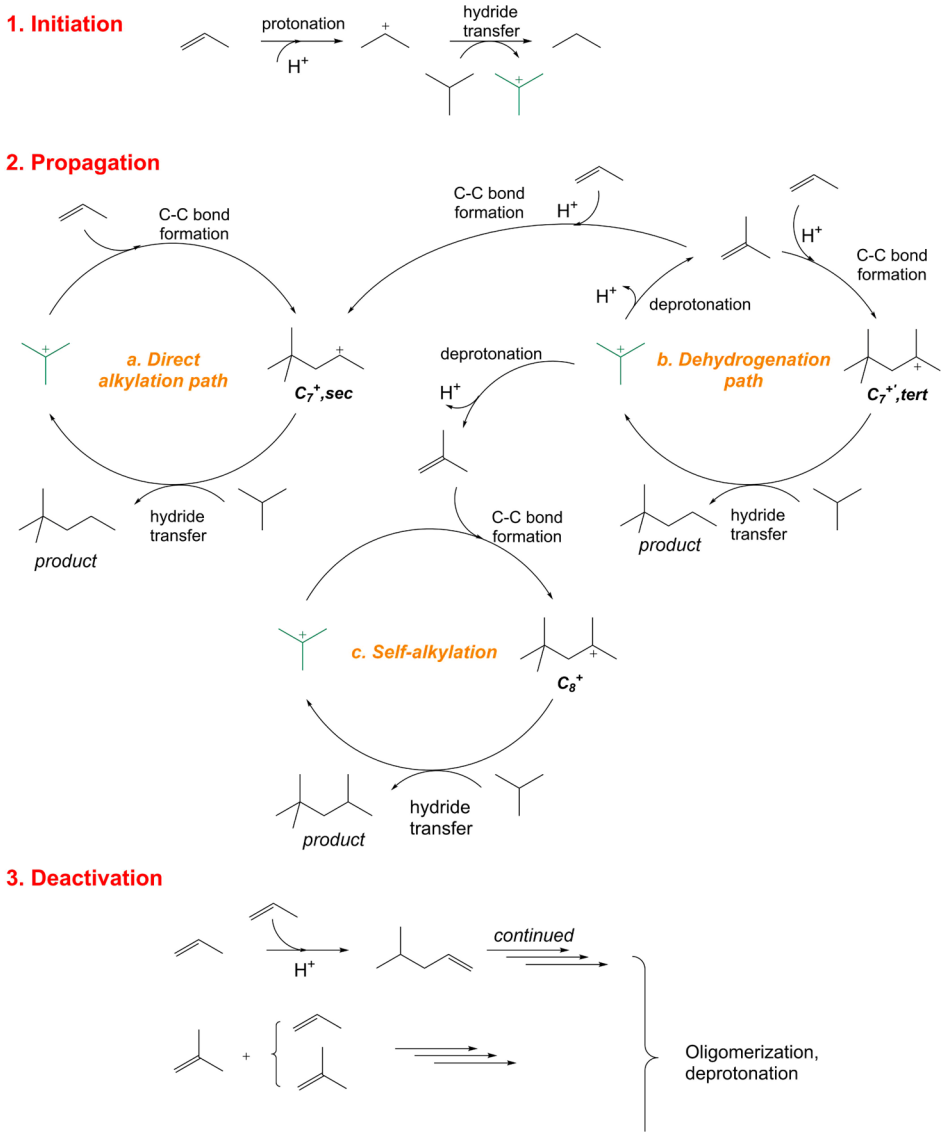

[a]The *tert*-butyl cations are indicated in green.

is also fundamental to catalyst deactivation of the alkylation reaction catalyzed by solid acids.[13] The understanding that reactive olefinic intermediates are the precursors of catalyst deactivation forms the basis of the hydrogenation regeneration cycle applied in AlkyClean technology,[14] which was jointly developed by CB&I, Albemarle Catalysts and Neste Oil. It is the world's first solid acid catalyst alkylation unit and was recently commissioned in China.[15] Understanding the complex mechanisms underlying the alkylation chemistry and competitive deactivation path is a crucial step toward further development and optimization of more sustainable and environmentally benign alkylation processes.

Alkylation reactions over solid acid catalysts usually give product distributions similar to those for the liquid acids, and there is a consensus that isobutane−alkene alkylation proceeds via intermediate carbenium ion formation in both homogeneous and heterogeneous applications.[16,17] Extensive studies on heterogeneously catalyzed alkylation processes over solid acids carried out during the last 25 years allowed formulation of the basic mechanisms of the formation of the desirable alkylate product and of the competing oligomerization reactions resulting in catalyst deactivation.[13,18−24] The alkylation process involves a complex network of catalytic reaction cycles with several feedback loops, where the initiation, propagation, and deactivation paths can be clearly distinguished (Scheme 1).[5,6,17,25−27] These reaction paths are intimately coupled. The catalytic process is initiated by the formation of *tert*-butyl cations via alkene protonation followed by a hydride transfer reaction with isobutane. This initiation process is taken over by propagation reactions. The acidic protons do not directly participate in the alkylation process, and the propagation cycle involves a continuous regeneration of carbocationic intermediates (e.g., *tert*-butyl or heptyl cations) acting as the confined organocatalysts. The key elementary reactions of the alkylation process are the hydride transfer reactions between isobutane and carbenium ion intermediate and the C−C bond formation between a *tert*-butyl cation and alkene. Deprotonation of these confined carbocations disrupts the propagation cycle and yields alkene byproducts contributing to the deactivating oligomerization paths. These result in a buildup of heavier compounds in

DOI: 10.1021/acscatal.7b02877
ACS Catal. 2017, 7, 8613−8627

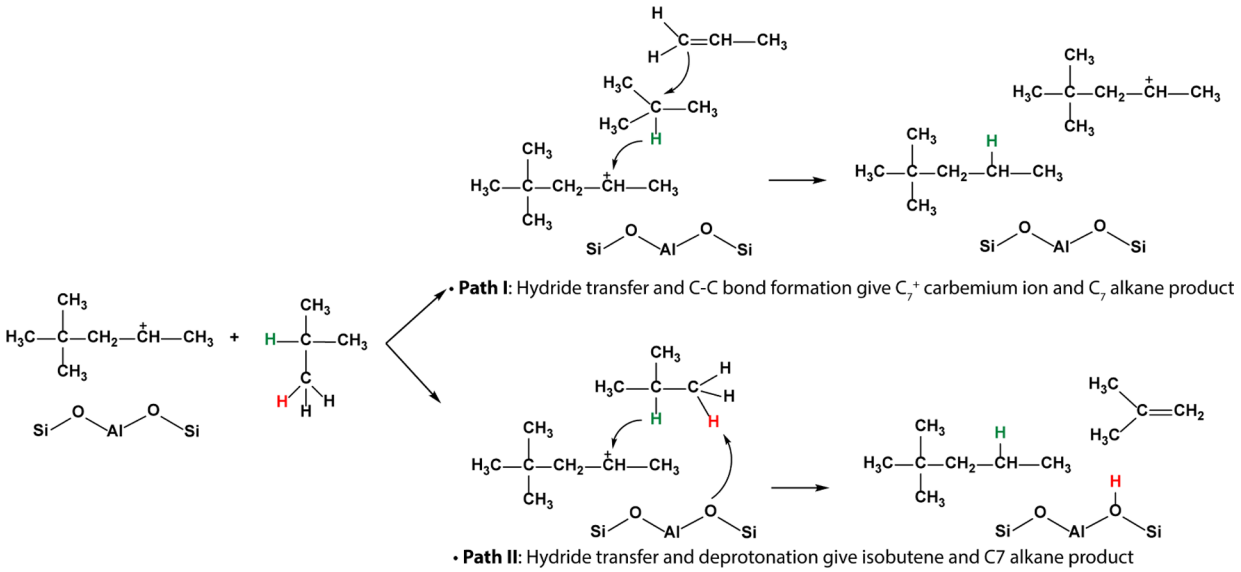

Figure 1. Schematic presentation of the two competitive hydride transfer reaction paths: hydride transfer synchronous with C−C bond formation (path I) versus isobutane dehydrogenation (path II).

zeolite nanopores, which can also undergo further transformations via hydride or proton transfer, cracking, or cyclization.[5] On the basis of experimental observations it has been suggested that the hydride transfer reaction has to be fast in comparison to the deactivating oligomerization paths to obtain a high alkylation yield.[3] The direct proton catalyzed C−H and C−C bond cleavage via carbonium ion intermediates does not contribute significantly to the overall performance[28,29] and will not be considered in this study. It will be shown computationally that the onset of the oligomerization can be postponed by suppressing the deprotonation of the carbenium ion intermediate.

Whereas protonation or deprotonation reactions of olefins and their oligomerization catalyzed by zeolites have been extensively studied before and the mechanistic details of these processes are well understood, this is not the case for the hydride transfer reactions.[30−32] Early computational studies on the mechanism of the hydride transfer were carried out by the groups of Kazansky, van Santen, and Corma in the late 90s.[33−37] Density functional theory (DFT) calculations by Kazansky et al.[33,34] on minimalistic cluster models considered the hydride transfer as the reverse reaction of the C−C bond cleavage, which occurs via a carbonium ion type high-energy transition state. Later DFT studies by Boronat et al.[35−37] based on the embedded cluster models of the zeolite acid sites provided a much reduced activation barrier for the hydride transfer between isobutane and *tert*-butyl cation with respect to the zeolite-bound alkoxy intermediate, bringing the computed values closer to the estimated barrier of 120 kJ/mol deduced from the experimental kinetics modeling.[38] Later, Neurock and co-workers[39,40] revisited the mechanism of the isobutane−butene alkylation on a phosphotungstic solid acid and the H-form of mordenite zeolite. Periodic DFT calculations revealed that the hydride transfer reaction from isobutane to the adsorbed alkoxy intermediate proceeds via a hydride-sharing cationic species that has to undergo a rotation, so that the positive charge which shifts in the complex by the hydride transfer reaction remains stabilized by the negative charge left on the deprotonated sold acid site. The essential contribution to the overall barrier for the hydride transfer step is the energy required to convert the adsorbed alkoxy species into a carbenium ion. The shift from the oversimplified cluster models to much more realistic and chemically representative periodic models reduced substantially the predicted barriers for the hydride transfer reactions.

In this work, we significantly extend our understanding of the isobutane−alkene alkylation mechanism on the basis of a detailed periodic DFT study using realistic zeolite models complemented by extended microkinetic modeling and Configuration-al-Bias Monte Carlo (CBMC)[41−43] simulations. In particular, the role of the difference in proton reactivity on the selectivity of the reaction is investigated. We select the alkylation of isobutane with propene rather than 2-butene as a model catalytic process to facilitate the product and reaction path analysis, as it reduces the number of involved reaction intermediates.

The DFT analysis of the reaction paths reveals two different hydride transfer reaction mechanisms (Figure 1). In the later microkinetic simulations we have included the two mechanistic paths for all hydride transfer reactions, as illustrated in Scheme 1. In path I the hydride transfer occurs in a three-molecule complex of "carbenium−isobutane−alkene". In case the carbocation is a heptyl cation and the alkene molecule is propene, the complex decomposes to product heptane and another heptyl cation. As we will see later, this has important consequences for the relative rates of the alkylate formation and carbocation deprotonation path. The other hydride transfer reaction mechanism (path II) does not involve a third molecule but requires a nearby Lewis basic site that can accept a proton. For this mechanism, the reaction of heptyl cation with isobutane yields heptane and an isobutene molecule. DFT calculations show that in this case the hydride transfer and the isobutene formation occur simultaneously. This is in line with the experimental observation by Lercher et al.[18] that, for the self-alkylation, the hydride transfer and the short alkane production are parallel. Microkinetic simulations indicate that path I dominates the hydride transfer mechanism under the catalytic conditions. Furthermore, these simulations show that,

DOI: 10.1021/acscatal.7b02877
ACS Catal. 2017, 7, 8613−8627

by varying the proton reactivity and the reaction conditions, the relative rates of the competitive reaction paths can be changed with large consequences for the selectivity and productivity of the overall alkylation process. Consistent with earlier experimental observations,[10,24,44] we will consider the ratio of alkylate production versus alkene production as a measure of catalyst alkylation productivity.

The manuscript is organized as follows. First, in Quantum Chemical Calculations on the Reaction Paths we discuss the computational models and results of the quantum chemical calculations on the reaction mechanisms with a particular focus on the hydride transfer reactions and other important relevant elementary steps. A complete list of quantum chemical results on which the microkinetic simulations are based is summarized in the Supporting Information. A comparison of the reactivity of zeolite catalysts with varying framework compositions is made to reveal the role of the density of Brønsted acid sites (BAS) and La promotion on changes in reaction paths and corresponding energies. The mechanistic discussion is followed by Microkinetic Simulations, which presents the results of microkinetic simulations based on the DFT-computed reaction energetics. The paper is concluded with Discussion and Conclusions. Details of DFT calculations, computational models, and microkinetic simulations can be found in Methods at the end of the paper.

2. QUANTUM CHEMICAL CALCULATIONS ON THE REACTION PATHS

2.1. Zeolite Models. Zeolites with medium or small pores are not suitable as alkylation catalysts because of the steric hindrance in the formation and diffusion of the bulky alkylates. High catalytic activity and sufficient stability in isobutane−alkene alkylation can only be achieved with large-pore zeolites (Figure 2a).[45,46] In particular, La-exchanged faujasites have been identified by the Lercher group as highly active alkylation catalysts because of their slower deactivation rate.[24,47−51] The main catalytic material to be investigated here is such a highly acidic La-promoted zeolite of the faujasite structure, which will be compared with zeolite models of the same topology but different chemical composition resulting in a lower proton reactivity. Prior physicochemical characterization and DFT calculations have demonstrated that La^{3+} ions in the La-promoted faujasites are predominantly stabilized within the sodalite cages in the form of multinuclear OH-bridged La clusters (Figure 2b,c) or as isolated La^{3+} at S_I sites in the hexagonal prisms.[50] The high alkylation activity of La-exchanged faujasite associated with the La clusters located in the sodalite cages will be shown to be due to its high proton reactivity so that the deprotonation of carbenium ions is suppressed.

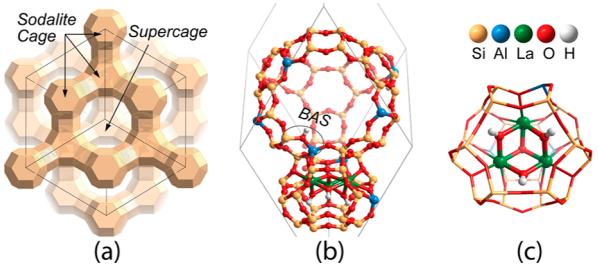

Figure 2. (a) Topology and channel connectivity of the faujasite-type zeolite structure and (b) atomistic model of the La-FAU zeolite containing the catalytic Brønsted acid sites (BAS) and exchangeable La cations in the form of (c) cationic La clusters ($[La_3O_4H_3]^{4+}$) confined inside the small sodalite cage.

Figure 2a shows the structure of a faujasite-type zeolite represented by large supercages connected through 12 ring channels. The periodic model used in our studies has a Si/Al ratio equal to 7. In the pure hydrogen FAU it contains six accessible Brønsted acid sites (BAS) within the supercage. The La-promoted La-FAU model contains a trinuclear hydroxylated La cluster ($[La_3O_4H_3]^{4+}$) inside the sodalite cage (Figure 2b,c) and has only two accessible BAS in the supercage. To understand better the promoting role of La, we extend our computational analysis with one additional structure, namely, the Na-FAU zeolite (Figure S1 in the Supporting Information). Similar to the case for La-FAU, the reactive supercage environment of the Na-FAU model contains only two BAS, while the La cluster is replaced by four Na^+ ions inside the sodalite cages.

From the basic kinetic considerations based on the reaction mechanism of Scheme 1 outlined in the previous section, an ideal alkylation system would be such that the rate of C−C bond formation betweena *tert*-butyl cation and propene ($r_{C+\text{-}C}$) is higher than the rates of the carbenium ion deprotonation steps ($r_{deprotonation}$). Furthermore, the hydride transfer reaction should be faster than (i) the homologation of the C_7^+ intermediates that is the C−C bond formation between C_7^+ and alkene and (ii) the C_7^+ deprotonation. Because alkene oligomerization is the main deactivating path, its rate ($r_{oligomerization}$) should be the lowest for the whole catalytic network. Thus, the order of the relative reaction rates in the ideal alkylation system should be $r_{hydride\ transfer} > r_{C+\text{-}C} > r_{deprotonation} > r_{oligomerization}$.

The relative rates depend strongly on the nature of the catalyst system and the reaction conditions, which as we will see later are usually far from the ideal trend. The chemical composition of the solid acid catalysts defines their acid−base characteristics. In general, a decreased proton reactivity/acidity results in the stabilization of the grafted alkoxy species and in an overall decrease of the catalytic reaction rates. Because of the concomitant increase in the zeolite lattice basicity, the relative rate for the deprotonation increases with respect to other steps of the catalytic process. The other factor that directly influences these relative rates is the nature of the carbenium ion intermediates. Protonation of small alkenes such as propene and butene gives primary or secondary alkoxy species as the stable intermediates with carbenium cations being the transition states. In contrast, tertiary carbenim ions are present at finite temperatures in the zeolites as the separated ion pairs so that they can relatively freely move inside the zeolite cavity.[52,53] The resulting entropy gain compensates for the enthalpic losses due to the absence of a covalent bond between the cationic carbon and the anionic zeolite lattice site.[54−57] In this study, such entropy effects are accounted for indirectly in the microkinetic modeling. In view of the complexity of the mechanistic paths considered here and given the expected similarities of the activation entropies for the elementary steps of similar nature, the pre-exponential factors were estimated on the basis of the available literature data as outlined in Methods.

2.2. Hydride Transfer. Figure 3 presents the DFT-optimized structures and computed energetics of the two hydride transfer paths (as illustrated in Figure 1) inside the micropores of La-FAU and FAU zeolites. In line with the earlier

DOI: 10.1021/acscatal.7b02877
ACS Catal. 2017, 7, 8613−8627

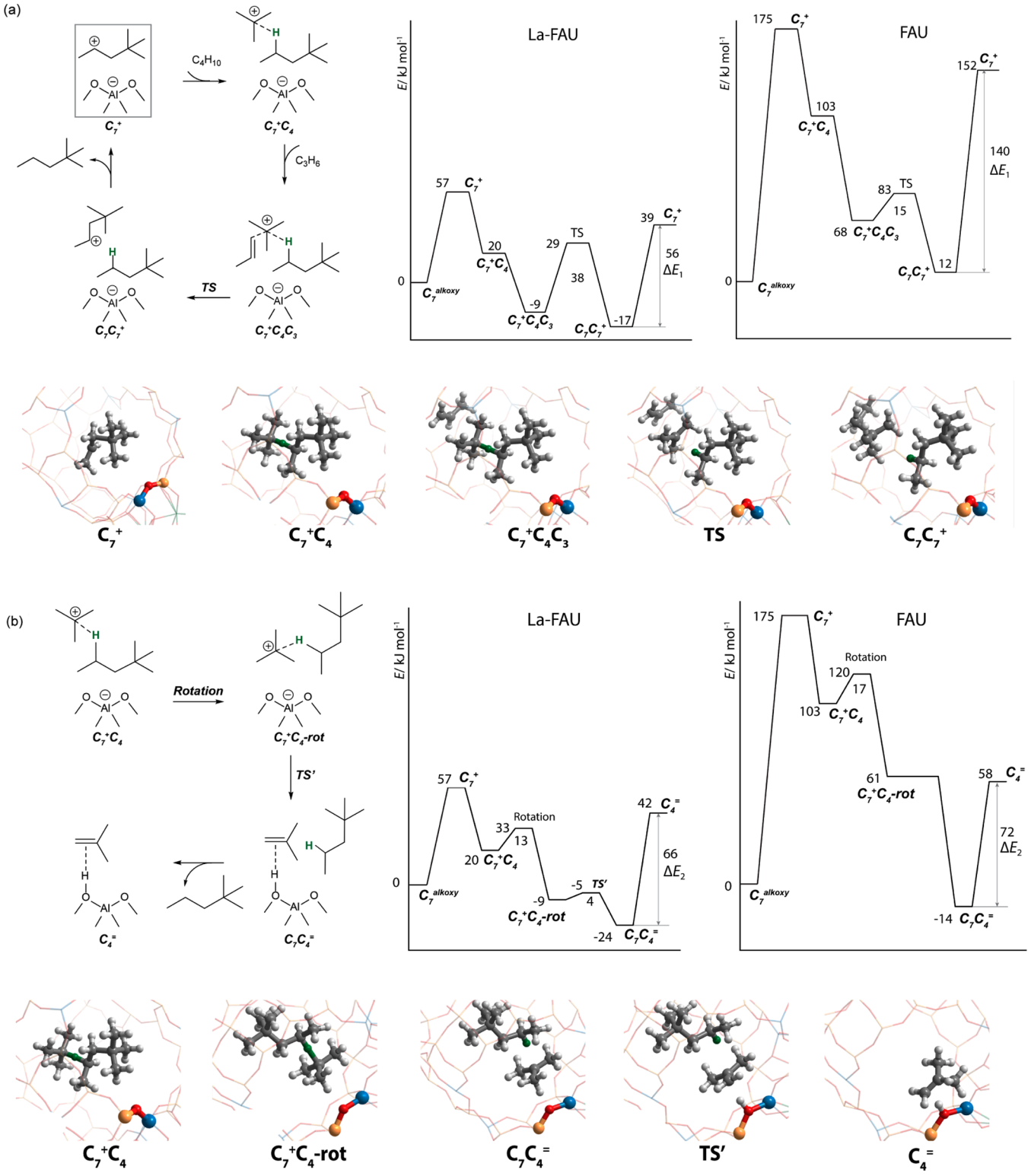

Figure 3. Reaction intermediates and transition states of the two hydride transfer reaction paths and comparison of the energetics on La-FAU and FAU: (a) propene-assisted hydride transfer synchronous with C−C bond formation (path I); (b) hydride transfer with isobutene formation (path II). The relative energies of reaction intermediates and transition states are with respect to the C_7 alkoxy species and the reactants adsorbed in the siliceous part of the zeolite framework. Illustration of the reaction intermediates and transition states: Si, yellow; Al, blue; O, red; H, white; C, gray. The transferred hydride is indicated in green.

mechanistic proposal of Neurock et al.,[39] our results show that the formation of the shared-hydride cationic complex is accompanied by its reorientation inside the zeolite void that allows optimization of its interaction with the negative charge on the zeolite framework. The C_7^+ carbenium ions can be part of transition states but can also be found as the local minima. The relative energies of these different states in Figure 3 are given with reference to the zeolite-grafted C_7 alkoxy

DOI: 10.1021/acscatal.7b02877
ACS Catal. 2017, 7, 8613−8627

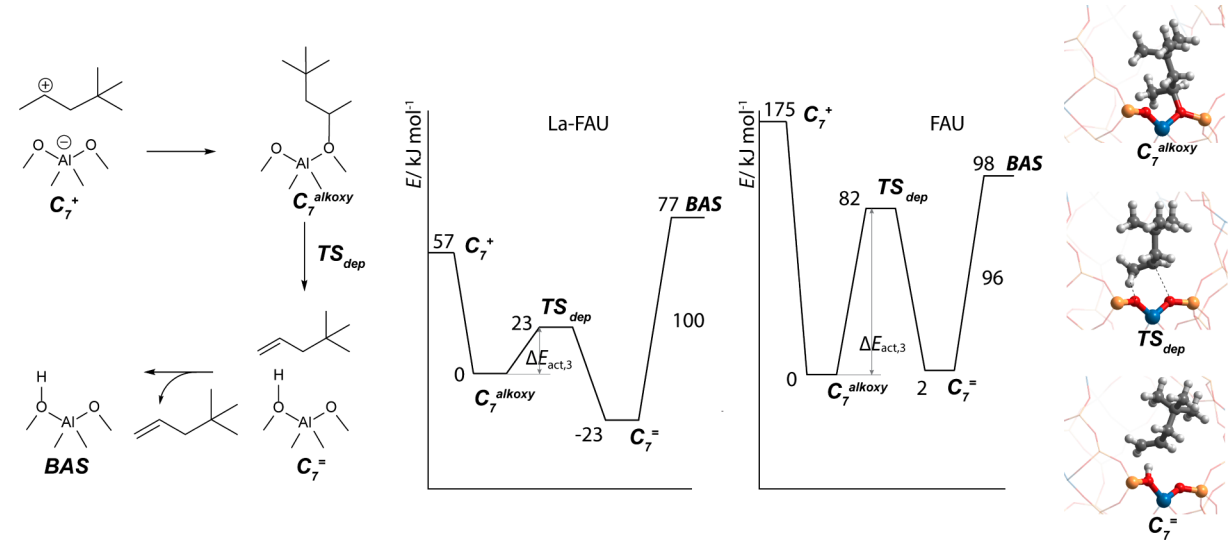

Figure 4. Reaction intermediates and transition states of C_7^+ deprotonation and comparison of the energetics on La-FAU and FAU. The relative energies of reaction intermediates and transition states are with respect to the C_7 alkoxy species in zeolites. Illustration of the reaction intermediates and transition states: Si, yellow; Al, blue; O, red; H, white; C, gray.

intermediate. Under the catalytic conditions, the C_7^+ carbenium ion is formed by the reaction of *tert*-butyl cation and propene (elementary steps are indicated in Scheme S2 in the Supporting Information). The cationic center on C_7^+ is directed away from the anionic site on the deprotonated zeolite lattice so that it can directly react with other substrates along the alkylation cycle. A side path toward the grafted C_7 alkoxy species requires a prior rotation of the carbocation inside the zeolite void.

The DFT results for the propene-assisted path (path I) are given in Figure 3a (Figure S2 in the Supporting Information). Path I is a subcycle that starts with a C_7^+ intermediate that forms a complex with isobutane and propene substrates. The interaction of isobutane with C_7^+ species forms the hydride-sharing complex $C_7^+C_4$, which after propene adsorption gives a precursor ($C_7^+C_4C_3$) for the hydride transfer process. Hydride transfer resulting in the decomposition of this complex closes the cycle, yielding the C_7 alkylate product and a new C_7^+ intermediate, which acts effectively as a confined organocatalyst. This cycle does not involve the formation of alkoxy intermediates. The stabilizing effect of the coadsorbed isobutane and propene on the C_7^+ intermediate is much stronger in FAU than in La-FAU (−107 vs −66 kJ/mol), evidencing an intrinsically lower stability of the C_7^+-containing ion pair formed inside the lanthanum-free FAU model. The subsequent hydride transfer step to give the C_7 alkane (2,2-dimethylpentane) proceeds with barriers of 15 and 38 kJ/mol for FAU and La-FAU catalysts, respectively. The main contribution to the energy barriers arises from the energy losses encountered upon the decomposition of the $C_7C_7^+$ complex, which is easier for the La-promoted system. This effect will be discussed in more detail in the next section. We will show that in comparison with FAU, the La-FAU supercage has a more efficient stabilization environment for the C_7^+ fragment that is left behind after the decomposition of the $C_7C_7^+$ complex.

The reaction intermediates and computed energy diagrams for the alternative bimolecular hydride transfer reaction (path II) simultaneously occurring with the deprotonation of *tert*-butyl cation are presented in Figure 3b (Figure S2 in the Supporting Information). The reaction starts with the rotation of the hydride-sharing $C_7^+C_4$ intermediate inside the supercage with estimated rotation barriers of 13 and 17 kJ/mol for La-FAU and FAU, respectively (Scheme S4 in the Supporting Information). These rotations stabilize the $C_7^+C_4$ cationic complex as it brings the C_4 fragment closer to the deprotonated lattice site, which provides better charge compensation. The hydride transfers partially to the C_7 moiety already upon the rotation, and it is completed upon further deprotonation of the C_4 fragment, resulting in a simultaneous formation of C_7 alkylate and isobutene coproduct. The deprotonation readily occurs when the methyl group of the *tert*-butyl fragment closely approaches the basic oxygens of the zeolite framework. The computed barriers for this step are negligible for both models, although the reaction in FAU is much more exothermic, evidencing the higher basicity of the unmodified faujasite lattice. Importantly, although in the La-FAU model the overall barriers for the two competing hydride transfer paths are very similar, the concerted bimolecular mechanism over La-free FAU proceeds with a barrier about half of that for the alternative propene-assisted hydride transfer reaction.

The C_7^+ cations are relatively large carbenium ions, so that the cumulative effect of the dispersion interactions with the zeolite walls is sufficient to make even the secondary carbocations stable in the geometries, when the cationic carbon is distantly situated from the localized negative framework charges of the deprotonated BAS. The transition states between C_7^+ and isobutane are more bulky and fill nearly completely the available space of the faujasite supercage. Hence, the alkylation reaction requires large cavities for space-unconstrained reactivity.

2.3. Deprotonation. For the deprotonation of C_7^+ cation, the hydrogen atom of the carbocation that is donated to the solid has to be close to the negatively charged oxygen atom associated with the deprotonated BAS. This geometrical constraint implies that prior to the deprotonation step a zeolite-bound alkoxy intermediate is formed, from which the proton is transferred to the zeolite lattice with a concomitant formation of the $C_7^=$ alkene product. The deprotonation energetics of the C_7^+ intermediates are illustrated in Figure 4. Counterintuitively, the activation energy for the deprotonation

DOI: 10.1021/acscatal.7b02877
ACS Catal. 2017, 7, 8613−8627

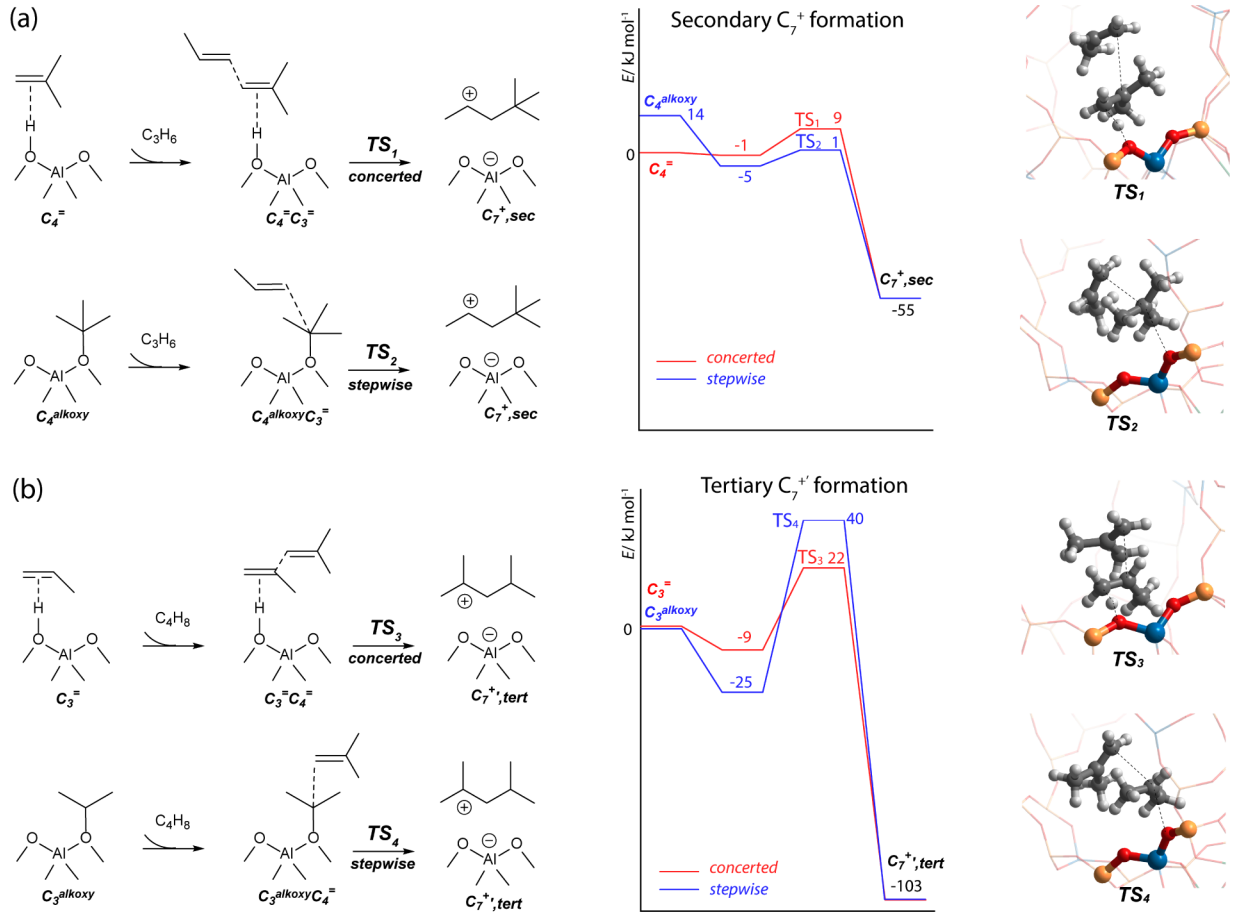

Figure 5. Reaction of isobutene and propene on BAS on La-FAU: (a) formation of secondary C_7^+ via protonated isobutene (corresponding product, 2,2-dimethylpentane); (b) formation of tertiary $C_7^{+\prime}$ via protonated propene (corresponding product, 2,4-dimethylpentane). The relative energies of reaction intermediates and transition states are with respect to the initially adsorbed π complexes of isobutene or propene and the reactants adsorbed in the siliceous part of the zeolite framework. Illustration of the transition states: Si, yellow; Al, blue; O, red; H, white; C, gray.

of the alkoxy intermediates is lower in the La-FAU with a higher proton reactivity than in FAU. This observation can be explained by the higher stability of the alkoxy intermediate bound to the more basic lattice of the La-free model, as is evidenced by the much lower exothermicity of the formation of the grafted C_7 alkoxy species from C_7^+ in La-FAU (−57 kJ/mol) than in FAU (−175 kJ/mol), in line with our previous proposal on the lower basicity of the deprotonated lattice of La-FAU in comparison with FAU.

Under the actual catalytic conditions, this deprotonation reaction has to compete with the hydride transfer and oligomerization paths. Only when the local isobutane concentration is sufficiently high will it bias the hydride transfer. As we will see from the microkinetic simulations, such conditions will effectively prevent the approach of C_7^+ cation to the localized negatively charged site of the zeolite framework. A similar effect is expected for the coupling reaction of C_7^+ with another propene molecule that will be the onset of the deactivation. The activation energy for such a reaction (Figure S3 in the Supporting Information) is slightly higher than that predicted for the deprotonation, suggesting the dominant role of the latter in the deactivation process.

Protonation of isobutene on a BAS of the zeolite regenerates the *tert*-butyl cation and brings the system back into the propagation cycle (Figure S4). There is a fast equilibrium between these two species in La-FAU zeolite. The estimated activation barrier for isobutene protonation to form *tert*-butyl cation is only 9 kJ/mol. The *tert*-butyl cation can be further transformed into a *tert*-butoxy intermediate with an activation barrier of 16 kJ/mol. When the transformation of adsorbed isobutene in La-free FAU zeolite is considered, the *tert*-butyl cation is more adequately described as a transition state on the potential energy surface formed with an activation barrier of 53 kJ/mol. The difference in the natures of the *tert*-butyl cation in La-FAU and FAU is the direct result of the difference in intrinsic zeolite acidity. The stronger acidity of La-FAU allows more effective stabilization of the *tert*-butyl state from a transition state into an intermediate, which is realized via a partial compensation of the excess lattice negative charge by the interaction with the cationic La complex. A similar lattice stabilization effect has also been observed for the H/D exchange reaction of benzene in extraframework Al-containing zeolites.[58] The protonation of isobutene to *tert*-butyl cation is much easier in more acidic La-FAU in comparison with FAU, and the weak acidity of zeolite only favors the formation of the π complex between BAS and isobutene.

2.4. C−C Bond Formation. The concerted hydride transfer and deprotonation of isobutane gives the byproduct isobutene, which can react with propene on BAS to form C_7^+ cations and produce C_7 alkylates via subsequent hydride transfer reactions. Depending on which alkene is protonated first, different C_7 isomers could be produced. The reaction of protonated

DOI: 10.1021/acscatal.7b02877
ACS Catal. 2017, 7, 8613−8627

Table 1. Comparison of Proton Activity as a Function of Faujasite Composition[a]

model	no. of protons per unit cell	$\Delta\nu(OH)_{CO_{ads}}$ (cm^{-1})	ΔE_{NH3}	ΔE_1 hydride transfer (path I)	ΔE_2 hydride transfer (path II)	$\Delta E_{act,3}$ deprotonation	$\Delta E_{act,4}$ oligomerization	$\Delta E_{act,5}$ dimerization
FAU	6	409	−125	140 (83)	72 (120)	82	110	124
Na-FAU	2	518	−139	69	68	50	62	86
La-FAU	2	625	−156	56 (29)	66 (33)	23	28	67

[a] ΔE_1 is the energy barrier required for the decomposition of the $C_7C_7^+$ complex in the hydride transfer path I as indicated in Figure 3a. $\Delta E_{act,2}$ is the energy barrier required for the desorption of C_7 alkane in the hydride transfer path II as indicated in Figure 3b. Values in parentheses are the energy barriers of hydride transfer with respect to the alkoxy species. $\Delta E_{act,3}$ is the activation barrier of C_7^+ deprotonation with respect to the C_7 alkoxy species as indicated in Figure 4. $\Delta E_{act,4}$ is the activation barrier of the oligomerization reaction between C_7^+ and propene with respect to the C_7 alkoxy species as indicated in Figure S3 in the Supporting Information. $\Delta E_{act,5}$ is the activation barrier for propene dimerization (reaction step of surface propoxy and propene). Energies are given in kJ/mol.

isobutene with propene forms a secondary C_7^+ similar to the propene-assisted hydride transfer path discussed above, with 2,2-dimethylpentane alkylate formed after the hydride transfer reaction. When isobutene reacts with the adsorbed propene that is the grafted propyl species, a tertiary $C_7^{+\prime}$ is produced, from which another C_7 isomer, namely 2,4-dimethylpentane, is formed after the hydride transfer. The reaction of isobutene and propene can proceed via concerted and stepwise mechanisms (Figure 5). The formation of secondary C_7^+ via the initial protonation of isobutene over La-FAU has activation barriers of 10 and 6 kJ/mol for concerted and stepwise mechanisms, respectively. The formation of tertiary $C_7^{+\prime}$ from protonated propene requires higher barriers of 31 and 65 kJ/mol for the concerted and stepwise mechanisms, respectively. These reactivity differences are attributed to the fact that the formation of secondary C_7^+ takes place via a transition state of the tertiary carbenium ion that is the protonated isobutene, which is more energetically favorable than the secondary carbenium ion (protonated propene) transition state involved in the formation of the tertiary $C_7^{+\prime}$. Thus, our calculations indicate that the formation of secondary C_7^+ corresponding to the product of 2,2-dimethylpentane is favored for the reaction of isobutene and propene over the alternative reaction channels. As the above stability considerations of carbocations are independent of the zeolite acid strength, the conclusion on the isomer selectivity holds for both La-FAU and FAU systems considered here.

Previous experimental studies identified 2,3-dimethylpentane as the main product of propene−isobutane alkylation[59−61] rather than the 2,2-dimethylpentane product which could be expected from the computational data presented thus far. This apparent inconsistency is related to the fast isomerization of the initially produced secondary C_7^+ (Figure S5 in the Supporting Information). This process starts with an intramolecular hydride shift, i.e. migration of a hydride ion from an adjacent carbon atom to the positive carbon center resulting in a metastable 2,2-dimethylpentyl(3) cation, which then undergoes an intramolecular methyl shift to produce a 2,3-dimethylpentyl(2) cation. This isomerization reaction is very fast and thermodynamically favorable, as it yields a very stable tertiary carbenium ion. For the La-FAU catalyst, DFT calculations predict the reaction to be exothermic by −68 kJ/mol and to proceed with a barrier of only 3 kJ/mol. The hydride transfer from isobutane to 2,3-dimethylpentyl(2) cation at the next step gives 2,3-dimethylpentane, in agreement with the experimental observations.

When isobutene acts as the alkylation reagent, the C_8 alkylate can be produced via the self-alkylation (path 2c, Scheme 1). The reactions of isobutene toward C_8^+ on the BAS in La-FAU show activation barriers of 8 and 6 kJ/mol for concerted and stepwise mechanisms, respectively (Scheme S8 in the Supporting Information). The hydride transfer between C_8^+ and isobutane yields the C_8 product, which is 2,2,4-trimethylpentane. As C_8^+ and tertiary $C_7^{+\prime}$ are structurally analogous, they show similar reactivity toward hydride transfer. Hydride transfer via the deprotonation path requires an activation barrier of 24 kJ/mol, and the alternative path accompanied by the formation of C−C bond between *tert*-butyl and propene has a barrier of 61 kJ/mol.

Several carbenium species are produced during the alkylation process, which upon the hydride transfer from isobutane produce the corresponding alkane products. We compare the reactivity of different carbenium ions toward hydride transfer as well as the reactivity of propene and isobutene as the alkylation reagents (Figure S6 in the Supporting Information). The interaction of a free carbenium with isobutane leads to the formation of the hydride-sharing complex, which could release the corresponding alkane via a concerted deprotonation/hydride transfer mechanism or via a path involving the assistance of another alkylation reagent molecule. The hydride transfer accompanied by C−C bond formation yields a secondary C_7^+ or a tertiary C_8^+ when propene or isobutene is used as the alkylation reagent. The C_6^+ and $C_7^+{}_{sec}$ show similar reactivity for hydride transfer, as they are both secondary carbeniums. Similar reactivity was also observed for the tertiary carbenium $C_7^+{}_{tert}$ and C_8^+. In general, the intrinsic activation barriers for hydride transfer with the secondary carbenium ions are lower than those with the tertiary ions for both propene and isobutene used as the alkylation reagents, implying higher reactivity of the secondary carbenium ions in comparison to that of the tertiary ions. Furthermore, for all of the carbenium ions, similar barriers of hydride transfer are predicted for both propene and isobutene alkylation reagents. However, the self-alkylation paths are generally more thermodynamically favorable because of the higher stability of the produced tertiary C_8^+ carbenium ions.

For a summary of the energetics of the complete reaction schemes of propene−isobutane alkylation we refer to the Supporting Information.

2.5. Proton Activity as a Function of Zeolite Composition. In this subsection we will discuss the change in the proton activity of different faujasite zeolites with varied chemical composition. Table 1 summarizes the computed energy parameters for the key competing reaction steps as well as the computed results of acidity probing for the selected zeolite models. Adsorptions of CO and NH_3 were used here as the acidity probes. The increased stretching frequency of CO and increased adsorption energy of ammonia indicates that La-FAU contains the most reactive protons. The DFT results show that the zeolite composition, and accordingly the reactivity of

DOI: 10.1021/acscatal.7b02877
ACS Catal. 2017, 7, 8613−8627

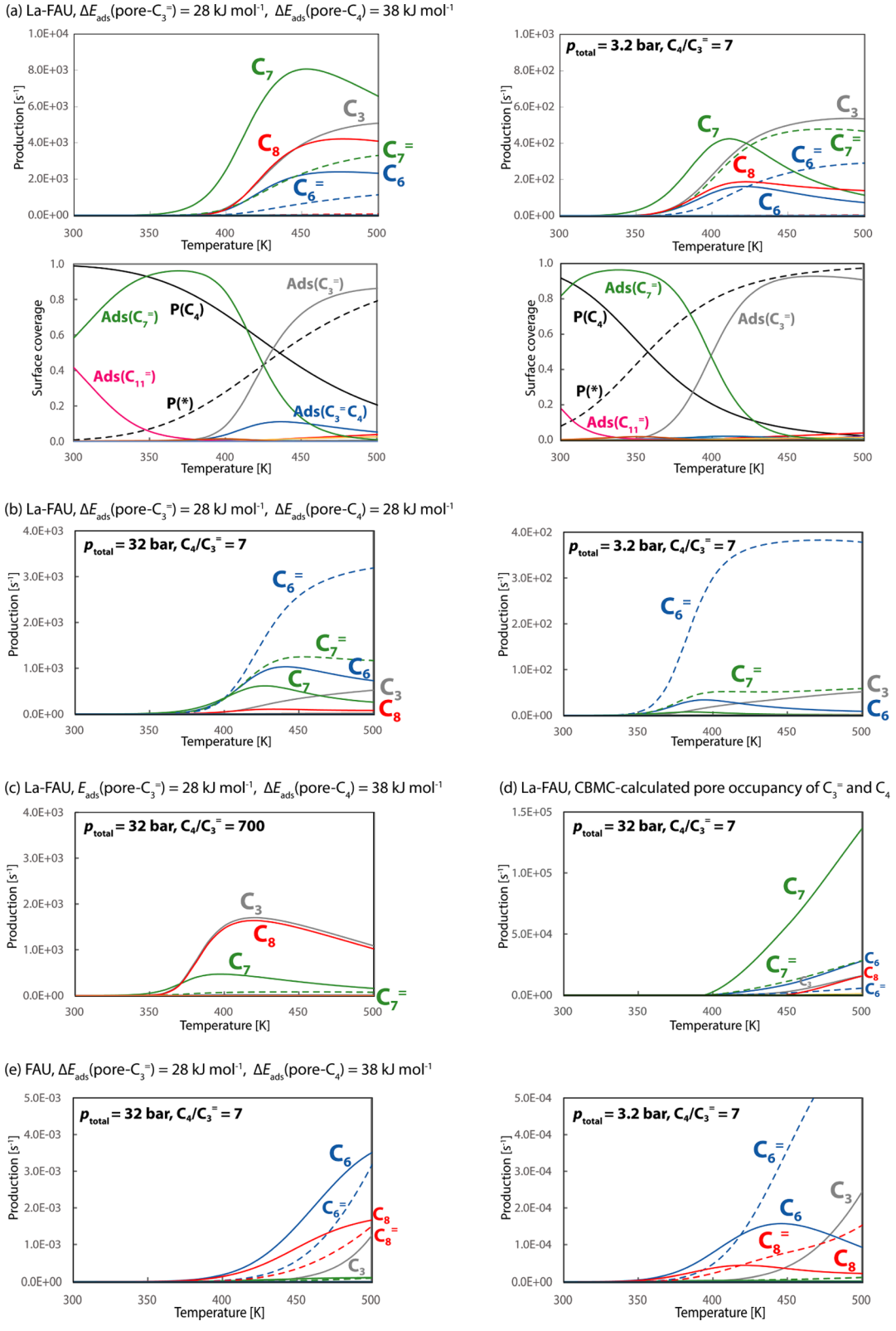

Figure 6. Microkinetics simulated production rates of the alkylation reaction at different value of total pressure as a function of temperature. (a) Predicated reaction rates on La-FAU model with corresponding surface coverages of intermediates below, using DFT-calculated adsorption energies of reactants in the proton-ree zeolite nanopores with values of ΔE_{ads}(pore-$C_3^=$) = 28 kJ mol^{-1}, and ΔE_{ads}(pore-C_4) = 38 kJ mol^{-1} ($C_4/C_3^=$ = 7). (b) Microkinetic simulations on La-FAU model with ΔE_{ads}(pore-$C_3^=$) = 28 kJ mol^{-1} and ΔE_{ads}(pore-C_4) = 28 kJ mol^{-1} ($C_4/C_3^=$ = 7). (c) Microkinetic simulations on La-FAU model with ΔE_{ads}(pore-$C_3^=$) = 28 kJ mol^{-1} and ΔE_{ads}(pore-C_4) = 38 kJ mol^{-1} ($C_4/C_3^=$ = 700). (d) Microkinetic simulations on La-FAU model with CBMC-calculated pore occupancy of propene and isobutane ($C_4/C_3^=$ = 7). (e) Microkinetic simulations on defect-free FAU model with ΔE_{ads}(pore-$C_3^=$) = 28 kJ mol^{-1} and ΔE_{ads}(pore-C_4) = 38 kJ mol^{-1} ($C_4/C_3^=$ = 7). In the plots of surface coverages, P(*) and P(C_4) indicate the pore occupancies of vacancy and isobutane and Ads($C_3^=$), Ads($C_7^=$), Ads($C_{11}^=$), and Ads($C_3^=C_4$) indicate the adsorption complexes of propene, heptene, undecene, and coadsorbed propene and isobutane on the BAS.

DOI: 10.1021/acscatal.7b02877
ACS Catal. 2017, 7, 8613−8627

its BAS, affects the relative preference of the hydride transfer reaction paths I and II. For the models FAU, La-FAU, and Na-FAU, all of the reaction barriers decrease with increasing acidity. For all of these aluminosilicate models DFT predicts higher activation energies for the elementary hydride transfer reaction steps than for the deprotonation reaction. However, mechanistic conclusions based on a direct comparison of activation barriers of elementary reactions has to be made with a certain amount of care, because of the strong dependence of the reaction conditions and resulting surface coverages expected for the apparent overall reaction rates. The catalytic cycles of hydride transfer and deprotonation involve several elementary reaction steps. In addition, all reaction steps are considered to be reversible so that they also become partially equilibrated. These effects are accounted for in the microkinetics simulations that are presented in the next section.

3. MICROKINETIC SIMULATIONS

To substantiate the above discussion and to get an insight into the effect of the reaction conditions on the catalytic networks discussed so far, we further constructed a microkinetic model based on the results of DFT calculations. Microkinetics simulations are necessary because product distributions illustrate that rate-controlling steps may change with zeolite composition as well as reaction conditions. The values of the activation energies in Table 1 already indicated differences in relative rates when zeolite composition varies. This becomes enhanced and sometimes altered when the effect of differences in local concentration at the reactive center are compared. The results of the microkinetics simulations that we present here have been obtained by solving the 107/77 ordinary differential equations (ODE) for La-FAU/FAU without assuming a rate-controlling step. For the extended details of the definition of the microkinetic model, including the key assumptions and the list of elementary reaction steps considered, we refer to Methods and the Supporting Information.

In the microkinetic simulations the adsorption of isobutane and propene is considered to occur on two types of sites: i.e., the siliceous wall and the Brønsted acidic protons. The propene and isobutane molecules are initially adsorbed from the gas phase to the siliceous zeolite walls and then readsorbed on the zeolite Brønsted acid sites (BAS). In the simulations the relative energies of adsorption on the proton sites are calculated with respect to the energy changes from the siliceous site to BAS. The adsorption of propene and isobutane at proton-free siliceous sites is approximated by the adsorption state in all-silica FAU. For each reactant, the calculated adsorption energies at the siliceous wall are similar for La-FAU, FAU, and all-silica FAU models, with $\Delta E(\text{pore-}C_3^=)$ of −31 to −28 kJ/mol and $\Delta E(\text{pore-}C_4)$ of −39 to −36 kJ/mol (Figure S7 and Table S1 in the Supporting Information). These values are in agreement with the experimental data of alkane adsorption on siliceous FAU, with a measured adsorption heat of 27 kJ/mol for propane and 33 kJ/mol for isobutane.[62] The adsorption of reactants to the BAS is stronger. The adsorption energies of isobutane from the siliceous wall to BAS change by −17 kJ/mol for both La-FAU and FAU, and the energy changes of adsorbed propene on BAS are more significant, with calculated values of −48 and −34 kJ/mol for La-FAU and FAU, respectively.

Figure 6 summarizes the most important results of microkinetics simulations for the La-FAU and FAU systems. For La-FAU (Figure 6a), at high pressure and low temperature, the C_7 alkylate is dominated by 2,2-dimethylpentane (which will rapidly isomerize to 2,3-dimethylpentane by a secondary reaction that is not included in the model) produced by the reaction of *tert*-butyl cation and propene. The negligible formation of 2,5-dimethylpentane from the reaction of isobutene and propyl cation is due to the lower stability of the *sec*-propyl cation in comparison to that of the *tert*-butyl cation. The second main products are C_8 and propane.

At higher temperatures the relative concentration of the alkenes increases. For the simulations carried out at a lower pressure, the product distributions change dramatically, resulting in the increase of the relative concentration of the alkene products. The main effect of elevated pressure is the reduction of the local concentration of propene, so that the deprotonation of C_7^+ carbenium ions and C_6 production become suppressed. This results in less alkene and more alkylated product, because isobutane suppresses propene adsorption. The minimum temperature of the reaction is determined by the desorption temperature of the $C_7^=$ molecules, which at a low temperature block the reaction site due to adsorption on the BAS. Self-alkylation is only found at elevated temperatures because of the further depletion of propene due to its increased consumption by the oligomerization reaction. The reaction of *tert*-butyl cation with isobutene then takes over and hydride transfer generates the C_8 self-alkylated product. Self-alkylation with C_8 coproduction occurs in parallel with undesirable C_3 and C_6 alkane formation, as predicted according to the Lercher mechanism.[18]

We next explored the effect of the varying adsorption energies of isobutane and propene on the results of the microkinetic modeling. The adsorption energy of isobutane ($\Delta E_{ads}(\text{pore-}C_4)$) was decreased from 38 to 28 kJ/mol (Figure 6b). In this case, the pore occupancy of isobutane is much lower in comparison to the previous case. For both pressure conditions, the $C_6^=$ and $C_7^=$ alkene products are the dominant products, with much less observed C_7 alkylate product. As the pore occupancy of isobutane is low, the hydride transfer is slow, resulting in very low C_7 alkylate production.

The production selectivity is also strongly affected by the substrate ratio in the hydrocarbon feed. When the ratio of isobutane and propene is increased from 7 to 700 at a total pressure of 32 bar, which resembles the state of minimized olefin concentration, the self-alkylated C_8 product becomes dominating with the coproduced propane (Figure 6c). As the production of C_7 and C_6 species requires propene, the formation of the related C_7 alkylate and alkene becomes strongly suppressed. In addition, negligible production of C_6 species was observed in this case. This agrees with the experimental observation[18] that self-alkylation takes over from production of C_7 species, when propene concentration becomes very low.

To more accurately account for the relative concentrations of reactants at the reaction center, we also simulated the adsorption isotherms of isobutane and propene in siliceous faujasite by the Configurational-Bias Monte Carlo (CBMC) method[41−43] (details in the Figure S8 and discussion in the Supporting Information). The deduced adsorption heats (Figure S9 in the Supporting Information) are in reasonable agreement with DFT-calculated values. The CBMC adsorption simulations of isobutane and propene mixture with a ratio of 7 (Figure S10 in the Supporting Information), the usually used experimental ratio, indicate that at high pressure there is strong competitive adsorption of isobutane and propene in the siliceous zeolite that suppresses propene adsorption (Figure

DOI: 10.1021/acscatal.7b02877
ACS Catal. 2017, 7, 8613−8627

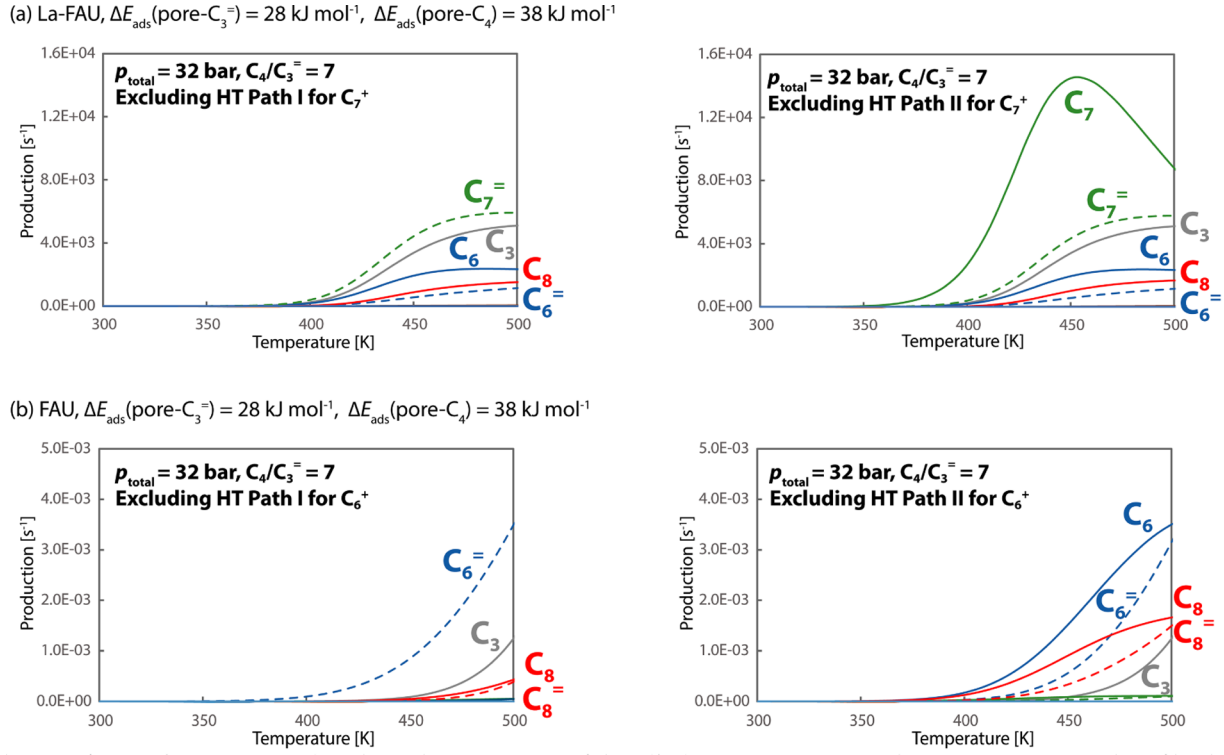

Figure 7. Dependence of microkinetics simulated production rates of the alkylation reaction on the two reaction paths of hydride transfer (HT). (a) Predicated reaction rates on La-FAU model excluding HT path I or path II for C_7^+. (b) Predicated reaction rates on FAU model excluding HT path I or path II for C_6^+.

S11 in the Supporting Information). In comparison with the results based on adsorption equilibria (Figure 6a, p_{total} = 32 bar), the reactant concentrations deduced from CBMC were also used in the microkinetic simulations (Table S2 in the Supporting Information), and the production rates in this case are qualitatively the same but with a predominance of production rate of C_7 alkylate (Figure 6d). This is due to the much higher pore occupancy of isobutane and suppression of propene adsorption (Figure S11a). This is one of the main reasons that alkylation by microporous zeolites has a high selectivity versus deactivating intermediates.

For FAU, only negligible C_7 alkylate production is observed (Figure 6e). At low temperature the main products are the self-alkylated C_8 molecule, hexane, and propane. At slightly higher temperatures alkene formation takes over. The main reason for C_8 instead of C_7 formation is depletion of propene due to rapid competing dimerization and rapid deprotonation of *tert*-butyl cation to give isobutene. The lower acidity makes the relative rate of deprotonation faster than in La-FAU, so that selectivity to alkene is larger. The strong acidity of zeolite catalyst is desired for the high C_7 alkylation activity, so that a high *tert*-butyl cation concentration is maintained during the catalytic propagation to produce alkylates.

The effect of the two hydride transfer reaction paths on the alkylation kinetics was studied by excluding one specific elementary step (Figure 7). One notes that omission of the elementary reactions that correspond to reaction path II has only a minor effect on the selectivity of the La-FAU system and no effect on that of the FAU zeolite. However, excluding the elementary reactions of hydride transfer path I leads to substantial losses of C_7 alkylate for La-FAU as well as C_6 production in FAU, which proves that path I is the dominant reaction for hydride transfer. The difference in kinetics of the La-FAU system versus that of the FAU system can be expressed as a difference in relative rates. In La-FAU one finds the relation $r_{C+\text{-}C} > r_{\text{hydride transfer}} > r_{\text{deprotonation}} > r_{\text{dimerization}}$, whereas in FAU this relation is $r_{\text{dimerization}} > r_{\text{hydride transfer}} \approx r_{\text{deprotonation}} > r_{C+\text{-}C}$. The inversion of the relative rates $r_{C+\text{-}C}$ and $r_{\text{dimerization}}$ is related to the increased instability of the carbenium ion versus its rate of deprotonation when proton reactivity decreases.

The difference in product distribution of La-FAU and FAU clearly indicates higher rates of oligomerization and deprotonation than hydride transfer in FAU in comparison to that in La-FAU. The self-alkylation reaction gives hexane as a coproduct for FAU while propane is the main coproduct for La-FAU. Hexane is generated by hydride transfer from an intermediate hexyl cation, formed by oligomerization of propene. This increased rate of propene oligomerization is the reason that propene is depleted and self-alkylation dominates for FAU. Experimentally, the oligomerization reaction leads to catalyst deactivation. The FAU result agrees with the experimental observation that self-alkylation increases with the onset of catalyst deactivation,[18] and the initially higher C_8 alkane concentration in comparison to that of $C_8^=$ alkene implies that hydride transfer is faster than the alkane deprotonation but less fast in comparison to La-FAU.

4. DISCUSSION AND CONCLUSIONS

The main chemical difference between La-FAU and FAU is the higher proton reactivity and higher negative zeolite framework charge of the former. It is generally found experimentally[13] that catalysts with strong Brønsted sites are most productive for the alkylation reaction versus oligomerization. Whereas our simulations do not explicitly consider the deactivation reactions, we observe a substantially increased relative propene

DOI: 10.1021/acscatal.7b02877
ACS Catal. 2017, 7, 8613−8627

dimerization rate and rate of alkene production for the model material with weaker BAS protons. An increased relative rate of oligomerization and alkene formation is experimentally found to be related to an increased rate of deactivation. We ascribe our model findings to the increased rate of deprotonation of the *tert*-butyl carbenium that is essential to maintain the alkylate-producing propagation cycle through C−C bond formation. This is not compensated by a relative increase in the rate of the hydride transfer reaction.

An important new result of the DFT calculations on chemically representative periodic models[63] is the finding of two types of hydride transfer reactions. We identified path I with a carbenium−isobutane−alkene complex intermediate. Hydride transfer is synchronous with C−C bond formation. Hydride transfer path II is a reaction between carbenium ion and isobutane. In this case proton back-donation to the zeolite occurs synchronously with hydride transfer. Then alkylate product and isobutene are primary products of this hydride transfer reaction. We find that hydride transfer reaction path I is the dominating path of the hydride transfer reaction.

In the deactivation reaction we did not explicitly study the formation of the final bulky carbocation products proposed by Lercher[24] and others[64] that consume protons by the pairing reaction and block zeolite micropore space. An estimate of the rate of deactivation can be made on the basis of the relative rates of propene oligomerization versus C_7 and C_8 product formation. A difference in rates of the factor 10 to 100 implies that deactivation will take place after ca. 10−1000 turnovers, which gives a deactivation rate estimate comparable to the values reported by Lercher and co-workers.[24] The exponential decrease in rate and the dominance of olefin oligomerization that they report imply that the hydride transfer becomes suppressed. This may be because site occupation by deactivating molecules in the same cavity leads to steric inhibition of the large reaction intermediates for hydride transfer. Indeed, the activation barriers of the hydride transfer reaction increase, as is confirmed by the results summarized in Figure 8. This increases the relative rate of the competing reactions of oligomerization and deprotonation. Deactivation effectively becomes an autocatalytic process. The loss of protons, due to deactivating proton consumption reactions,[65] will also increase the negative charge of the zeolite framework, contributing to an increase in the rate of the deprotonation reaction.

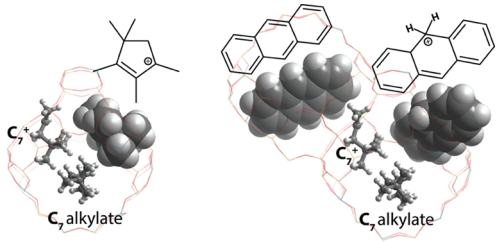

Hydride transfer / path I

Model	ΔE_1, kJ/mol
La-FAU	56
La-FAU-Cyc	77
La-FAU-Ant	74

Figure 8. Effect of deactivating (model) carbonaceous deposits inside the zeolite cage on the activation barrier of the hydride transfer.

The current mechanistic findings impose conflicting requirements on the geometrical demands to the micropore structure that would give the optimum alkylation rates. Due to the size of the hydride transfer complex of isobutane and carbenium ions, a zeolite structure with large pore size should be beneficial. This also decreases the probability of the carbenium ion to approach the zeolite negative framework site necessary for proton back-donation and the generation of deactivating alkenes. The microkinetic simulations indicate the importance of high isobutane occupation of the zeolite micropores and the importance of competitive adsorption of olefin. In order to bias the relative rate of the hydride transfer reaction, a high isobutane concentration near the reaction center is needed. This requirement would be optimally realized for the small-pore zeolites, in which the local isobutane concentration would be increased through strong physical adsorption due to confinement. These conflicting requirements on pore size dimension suggest that a bimodal channel structure should be looked for in an optimal catalyst. An indication that alternative channel structure structures provide a better performance is the report that zeolite beta is a more stable catalyst for the alkylation reaction.[22]

The strong intrinsic acidity of zeolitic protons is essential for a good alkylation catalyst. A stable catalytic subcycle of alkylate formation requires stabilization of the carbenium ion intermediates. A low proton site concentration but a relatively high as well as delocalized negative charge as present in La-FAU is favorable. These help to stabilize the positive charge on the carbenium ion away from the proton acceptance site. Ways to alter the negative charge on the framework and to increase its negative polarity could be investigated by substitution of part of the Al in the aluminosilicate framework by Ga or Fe or partial replacement of Si by Ge.

In summary, we have employed theoretical approaches to carry out a comprehensive study of the complex reaction networks underlying the alkylation process by zeolite solid acid catalysts. The complex reaction mechanism of the isobutane−propene alkylation is discussed in full detail, on the basis of a complete analysis of computed reaction intermediates and extended microkinetic simulations without an a priori choice of rate-limiting elementary reaction steps. It is shown that when the hydride ion is transferred to a carbenium ion it requires a complex of three molecules: isobutane, carbenium ion, and additional olefin, and bond cleavage and bond formation reactions occur simultaneously. Alternatively, hydride transfer between isobutane and carbenium ion occurs in concert with proton back-donation to the zeolite framework, by which the isobutane is converted into isobutene. A high selectivity of alkylated product requires strong competition of the hydride transfer reactions versus deprotonation of the carbenium ion intermediates. Oligomerization of alkenes is the main reaction that deactivates the catalysts. The deprotonation reaction is suppressed by solid acids with strongly acidic protons and delocalized framework negative charge that stabilize the large intermediate carbenium ions. The role of the zeolite nanopores is also essential because they increase the local concentration of adsorbed isobutane, necessary for efficient hydride transfer, which counteracts the undesirable deprotonation reaction of the carbenium intermediates.

DOI: 10.1021/acscatal.7b02877
ACS Catal. 2017, 7, 8613−8627

5. METHODS

5.1. DFT Calculations. All periodic DFT calculations were performed using VASP with the Perdew−Burke−Ernzerhof (PBE) functional.[66−70] The projected augmented waves (PAW) method was used to describe the electron−ion interactions.[71,72] The cutoff energy of the plane waves was set to 500 eV. Brillouin zone sampling was restricted to the Γ point.[73] Convergence was assumed to be reached when the forces on each atom were below 0.05 eV/Å. A modest Gaussian smearing of 0.05 eV was applied to band occupations around the Fermi level, and the total energies were extrapolated to $\sigma \rightarrow 0$. van der Waals interactions were described by the dispersion-corrected DFT-D3 method with Becke−Jonson damping.[74] The climbing image nudged elastic band (CI-NEB) method was used to determine the minimum energy path and to locate the transition state structures.[75] The maximum energy geometries along the reaction path obtained with the CI-NEB method were further optimized using a quasi-Newton algorithm. The highest energy structures located along the reaction coordinate were referred to as transition states, although their nature was not confirmed through vibrational analysis. The reaction coordinate for hydride transfer over zeolites is known to be extremely flat, making it difficult to isolate the true transition state. These aspects have been fully discussed by Neurock et al. in ref 39. The energetics of the reaction intermediates and transition states were directly obtained from DFT-D3 calculations without further thermal corrections.

5.2. Computational Models. The rhombohedral faujasite unit cell with periodic boundary condition was used as a computational model.[76] The cell parameters were optimized for the defect-free faujasite model (FAU) with an Si/Al ratio of 7. The FAU model contains six framework Al atoms in the unit cell with charge-compensating protons at O1 positions. The optimized lattice parameters are $a = b = c = 17.44$ Å and $\alpha = \beta = \gamma = 60°$. The La-containing faujasite (La-FAU) contains $[La_3O_4H_3]^{4+}$ in a sodalite cage with vicinal supercage BAS (Figure 2).[50] The positive charge of the La cluster was compensated by substituting four protons in the FAU model, and the zeolite models were always kept neutral. Full geometry optimizations with $[La_3O_4H_3]^{4+}$ and adsorbates were performed with fixed cell parameters. The Na-FAU model was built by replacement of the La cluster with four Na cations, located in the sodalite cage's 6 rings facing the hexagonal prisms which connect sodalite cages (Figure S1 in the Supporting Information).

5.3. Microkinetic Simulations. The corresponding ordinary differential equations for the alkylation reaction rates have been solved under steady-state conditions by employing the in-house-developed C++ program MKMCXX.[77] The reaction rate for the forward and backward elementary step is expressed using the Arrhenius equation:

$$k = A \exp\left(\frac{-E_a}{RT}\right)$$

where A stands for the pre-exponent and E_a, R, and T refer to the activation barrier, gas constant, and temperature, respectively. The pre-exponents of propene and isobutane adsorption/desorption were estimated from the calculated adsorption entropies by De Moor et al.[78,79] (Table S3 in the Supporting Information), with values of $10^{10}/10^{16}$ s^{-1} for adsorption/desorption. To take account of a small diffusion constant barrier, an activation barrier of 10 kJ/mol was used for the adsorption from the gas phase to zeolite micropores.[80] As the entropy losses are higher for products with greater carbon numbers, the (re)adsorption and desorption of these products were considered with estimated pre-exponents of $10^9/10^{17}$ s^{-1}, to correct for respective entropy loss and gain. For surface reactions, we have used the rule that formation of an alkoxy species decreases the activation entropies further by the same amount (pre-exponents of $10^9/10^{17}$ s^{-1}) and that activation entropies do not vary between the physically adsorbed and transition states (pre-exponents of $10^{13}/10^{13}$ s^{-1}) except for association and dissociation reactions that are chosen to have the same pre-exponent differences as those between adsorption and desorption ($10^9/10^{17}$ s^{-1}). These are reasonable approximations that are of the same order of magnitude as found in the literature. These approximations imply that we ignore differences in the pre-exponents that arise due to size or shape differences of the reaction.[55,56,81,82] With these assumptions we take account of the change in degrees of freedom in the respective reactions considered but assume the pores to be wide enough that there is no steric inhibition to their movement.

■ ASSOCIATED CONTENT

Supporting Information

The Supporting Information is available free of charge on the ACS Publications website at DOI: 10.1021/acscatal.7b02877.

Full reaction network of propene−isobutane alkylation, details of CBMC simulations, and additional supporting data (PDF)

■ AUTHOR INFORMATION

Corresponding Authors

*E-mail for R.A.v.S.: r.a.v.santen@tue.nl.
*E-mail for E.A.P.: e.a.pidko@tue.nl; e.a.pidko@tudelft.nl.

ORCID

Chong Liu: 0000-0003-0311-8744
Ali Poursaeidesfahani: 0000-0002-9142-206X
Thijs J. H. Vlugt: 0000-0003-3059-8712
Evgeny A. Pidko: 0000-0001-9242-9901
Emiel J. M. Hensen: 0000-0002-9754-2417

Present Address

⊥Inorganic Systems Engineering group, Department of Chemical Engineering, Delft University of Technology, Van der Maasweg 9, 2629 HZ Delft, The Netherlands.

Notes

The authors declare no competing financial interest.

■ ACKNOWLEDGMENTS

C.L. thanks China Scholarship Council (CSC) for financial support. The Netherlands Organization for Scientific Research (NWO) is acknowledged for providing access to the supercomputer facilities. T.J.H.V acknowledges NWO−CW for a VICI grant. E.A.P. acknowledges support from the Ministry of Education and Science of Russian Federation (Project 11.1706.2017/4.6). The authors thank Mr. Bart Zijlstra and dr. Ivo Filot for technical assistance with the microkinetics simulations. The authors acknowledge the support from The Netherlands Center for Multiscale Catalytic Energy Conversion (MCEC). R.A.v.S acknowledges discussion with J. A. Lercher during his stay at TUM as advanced institute scholar.

DOI: 10.1021/acscatal.7b02877
ACS Catal. 2017, 7, 8613−8627

REFERENCES

(1) Corma, A. *Chem. Rev.* **1995**, *95*, 559−614.
(2) Bibby, D. M.; Howe, R. F.; McLellan, G. D. *Appl. Catal., A* **1992**, *93*, 1−34.
(3) Corma, A.; Martínez, A. *Catal. Rev.: Sci. Eng.* **1993**, *35*, 483−570.
(4) Martínez, A.; Corma, A.; Prieto, G.; Arribas, M. A. In *Encyclopedia of Catalysis*; Wiley: Hoboken, NJ, 2002.
(5) Feller, A.; Lercher, J. A. *Adv. Catal.* **2004**, *48*, 229.
(6) Traa, Y.; Weitkamp, J. In *Handbook of Heterogeneous Catalysis*; Wiley-VCH: Weinheim, Germany, 2008.
(7) Wang, H.; Meng, X.; Zhao, G.; Zhang, S. *Green Chem.* **2017**, *19*, 1462−1489.
(8) Ono, Y. *Catal. Today* **2003**, *81*, 3−16.
(9) Sanchez-Castillo, M. A.; Madon, R. J.; Dumesic, J. A. *J. Phys. Chem. B* **2005**, *109*, 2164−2175.
(10) Corma, A.; Miguel, P. J.; Orchillés, A. V. *Appl. Catal., A* **1996**, *138*, 57−73.
(11) Martínez-Espín, J. S.; De Wispelaere, K.; Janssens, T. V. W.; Svelle, S.; Lillerud, K. P.; Beato, P.; Van Speybroeck, V.; Olsbye, U. *ACS Catal.* **2017**, *7*, 5773−5780.
(12) Müller, S.; Liu, Y.; Kirchberger, F. M.; Tonigold, M.; Sanchez-Sanchez, M.; Lercher, J. A. *J. Am. Chem. Soc.* **2016**, *138*, 15994−16003.
(13) Corma, A.; Martinez, A.; Martinez, C. *J. Catal.* **1994**, *146*, 185−192.
(14) D'Amico, V. J.; van Broekhoven, E. H.; Nat, P. J.; Nousiainen, E. H.; Jakkula, J. NPRA Annual refining meeting, San Antonio, TX, Mar 17, 2002.
(15) http://www.hydrocarbonprocessing.com/news/2015/12/china-s-wonfull-starts-up-world-s-first-solid-acid-catalyst-alkylation-unit (accessed May 19, 2017).
(16) Kazansky, V. B. *Catal. Today* **1999**, *51*, 419−434.
(17) Schmerling, L. *J. Am. Chem. Soc.* **1945**, *67*, 1778−1783.
(18) Feller, A.; Guzman, A.; Zuazo, I.; Lercher, J. A. *J. Catal.* **2004**, *224*, 80−93.
(19) Corma, A.; Juanrajadell, M. I.; Lopeznieto, J. M.; Martinez, A.; Martinez, C. *Appl. Catal., A* **1994**, *111*, 175−189.
(20) Platon, A.; Thomson, W. J. *Appl. Catal., A* **2005**, *282*, 93−100.
(21) Simpson, M. F.; Wei, J.; Sundaresan, S. *Ind. Eng. Chem. Res.* **1996**, *35*, 3861−3873.
(22) de Jong, K. P.; Mesters, C. M. A. M.; Peferoen, D. G. R.; van Brugge, P. T. M.; de Groot, C. *Chem. Eng. Sci.* **1996**, *51*, 2053−2060.
(23) Weitkamp, J.; Traa, Y. *Catal. Today* **1999**, *49*, 193−199.
(24) Feller, A.; Barth, J.-O.; Guzman, A.; Zuazo, I.; Lercher, J. A. *J. Catal.* **2003**, *220*, 192−206.
(25) Schmerling, L. *J. Am. Chem. Soc.* **1946**, *68*, 275−281.
(26) Otvos, J. W.; Stevenson, D. P.; Wagner, C. D.; Beeck, O. *J. Am. Chem. Soc.* **1951**, *73*, 5741−5746.
(27) Gates, B. C.; Katzer, J. R.; Schuit, G. C. A. *Chemistry of Catalytic Processes*; McGraw-Hill: New York, 1979.
(28) Weitkamp, J.; Jacobs, P. A.; Martens, J. A. *Appl. Catal.* **1983**, *8*, 123−141.
(29) Narbeshuber, T. F.; Vinek, H.; Lercher, J. A. *J. Catal.* **1995**, *157*, 388−395.
(30) Bell, A. T.; Head-Gordon, M. *Annu. Rev. Chem. Biomol. Eng.* **2011**, *2*, 453−477.
(31) Van Speybroeck, V.; Hemelsoet, K.; Joos, L.; Waroquier, M.; Bell, R. G.; Catlow, C. R. A. *Chem. Soc. Rev.* **2015**, *44*, 7044−7111.
(32) van Santen, R. A. In *Modern Heterogeneous Catalysis*; Wiley-VCH: Weinheim, Germany, 2017; p 345.
(33) Kazansky, V. B.; Frash, M. V.; van Santen, R. A. *Catal. Lett.* **1997**, *48*, 61−67.
(34) Frash, M. V.; Solkan, V. N.; Kazansky, V. B. *J. Chem. Soc., Faraday Trans.* **1997**, *93*, 515−520.
(35) Boronat, M.; Viruela, P.; Corma, A. *J. Phys. Chem. A* **1998**, *102*, 9863−9868.
(36) Boronat, M.; Viruela, P.; Corma, A. *J. Phys. Chem. B* **1999**, *103*, 7809−7821.
(37) Boronat, M.; Viruela, P.; Corma, A. *Phys. Chem. Chem. Phys.* **2000**, *2*, 3327−3333.
(38) Yaluris, G.; Rekoske, J. E.; Aparicio, L. M.; Madon, R. J.; Dumesic, J. A. *J. Catal.* **1995**, *153*, 54−64.
(39) Janik, M. J.; Davis, R. J.; Neurock, M. *J. Catal.* **2006**, *244*, 65−77.
(40) Mullen, G. M.; Janik, M. J. *ACS Catal.* **2011**, *1*, 105−115.
(41) Vlugt, T. J. H.; Krishna, R.; Smit, B. *J. Phys. Chem. B* **1999**, *103*, 1102−1118.
(42) Dubbeldam, D.; Calero, S.; Vlugt, T. J. H.; Krishna, R.; Maesen, T. L. M.; Smit, B. *J. Phys. Chem. B* **2004**, *108*, 12301−12313.
(43) Vlugt, T. J. H.; García-Pérez, E.; Dubbeldam, D.; Ban, S.; Calero, S. *J. Chem. Theory Comput.* **2008**, *4*, 1107−1118.
(44) Weitkamp, J.; Maixner, S. *Zeolites* **1987**, *7*, 6−8.
(45) Chu, Y. F.; Chester, A. W. *Zeolites* **1986**, *6*, 195−200.
(46) Corma, A.; Martinez, A.; Martinez, C. *Catal. Lett.* **1994**, *28*, 187−201.
(47) Guzman, A.; Zuazo, I.; Feller, A.; Olindo, R.; Sievers, C.; Lercher, J. A. *Microporous Mesoporous Mater.* **2005**, *83*, 309−318.
(48) Lercher, J. A.; Feller, A.; Gaab, S. U.S. Patent 7,459,412, 2008.
(49) Sievers, C.; Liebert, J. S.; Stratmann, M. M.; Olindo, R.; Lercher, J. A. *Appl. Catal., A* **2008**, *336*, 89−100.
(50) Schüßler, F.; Pidko, E. A.; Kolvenbach, R.; Sievers, C.; Hensen, E. J. M.; van Santen, R. A.; Lercher, J. A. *J. Phys. Chem. C* **2011**, *115*, 21763−21776.
(51) Schüßler, F.; Schallmoser, S.; Shi, H.; Haller, G. L.; Ember, E.; Lercher, J. A. *ACS Catal.* **2014**, *4*, 1743−1752.
(52) Tuma, C.; Sauer, J. *Phys. Chem. Chem. Phys.* **2006**, *8*, 3955−3965.
(53) Piccini, G.; Alessio, M.; Sauer, J. *Angew. Chem., Int. Ed.* **2016**, *55*, 5235−5237.
(54) Tuma, C.; Sauer, J. *Angew. Chem., Int. Ed.* **2005**, *44*, 4769−4771.
(55) Gounder, R.; Iglesia, E. *Acc. Chem. Res.* **2012**, *45*, 229−238.
(56) Van der Mynsbrugge, J.; De Ridder, J.; Hemelsoet, K.; Waroquier, M.; Van Speybroeck, V. *Chem. - Eur. J.* **2013**, *19*, 11568−11576.
(57) Sarazen, M. L.; Iglesia, E. *Proc. Natl. Acad. Sci. U. S. A.* **2017**, *114*, E3900−E3908.
(58) Liu, C.; Li, G.; Hensen, E. J. M.; Pidko, E. A. *J. Catal.* **2016**, *344*, 570−577.
(59) Cardona, F.; Gnep, N. S.; Guisnet, M.; Szabo, G.; Nascimento, P. *Appl. Catal., A* **1995**, *128*, 243−257.
(60) Guisnet, M.; Gnep, N. S. *Appl. Catal., A* **1996**, *146*, 33−64.
(61) Nivarthy, G. S.; Feller, A.; Seshan, K.; Lercher, J. A. *Microporous Mesoporous Mater.* **2000**, *35*−*36*, 75−87.
(62) Eder, F.; Lercher, J. A. *Zeolites* **1997**, *18*, 75−81.
(63) Pidko, E. A. *ACS Catal.* **2017**, *7*, 4230−4234.
(64) Yarulina, I.; Goetze, J.; Gucuyener, C.; van Thiel, L.; Dikhtiarenko, A.; Ruiz-Martinez, J.; Weckhuysen, B. M.; Gascon, J.; Kapteijn, F. *Catal. Sci. Technol.* **2016**, *6*, 2663−2678.
(65) Haw, J. F.; Song, W.; Marcus, D. M.; Nicholas, J. B. *Acc. Chem. Res.* **2003**, *36*, 317−326.
(66) Kresse, G.; Hafner, J. *Phys. Rev. B: Condens. Matter Mater. Phys.* **1993**, *48*, 13115−13118.
(67) Kresse, G.; Hafner, J. *Phys. Rev. B: Condens. Matter Mater. Phys.* **1994**, *49*, 14251−14269.
(68) Kresse, G.; Furthmüller, J. *Phys. Rev. B: Condens. Matter Mater. Phys.* **1996**, *54*, 11169−11186.
(69) Kresse, G.; Furthmüller, J. *Comput. Mater. Sci.* **1996**, *6*, 15−50.
(70) Perdew, J. P.; Burke, K.; Ernzerhof, M. *Phys. Rev. Lett.* **1996**, *77*, 3865−3868.
(71) Blöchl, P. E. *Phys. Rev. B: Condens. Matter Mater. Phys.* **1994**, *50*, 17953−17979.
(72) Kresse, G.; Joubert, D. *Phys. Rev. B: Condens. Matter Mater. Phys.* **1999**, *59*, 1758−1775.
(73) Monkhorst, H. J.; Pack, J. D. *Phys. Rev. B* **1976**, *13*, 5188−5192.
(74) Grimme, S.; Ehrlich, S.; Goerigk, L. *J. Comput. Chem.* **2011**, *32*, 1456−1465.
(75) Henkelman, G.; Jónsson, H. *J. Chem. Phys.* **2000**, *113*, 9978−9985.
(76) Hriljac, J. A.; Eddy, M. M.; Cheetham, A. K.; Donohue, J. A.; Ray, G. J. *J. Solid State Chem.* **1993**, *106*, 66−72.

DOI: 10.1021/acscatal.7b02877
ACS Catal. 2017, 7, 8613−8627

(77) Filot, I. A. W.; Zijlstra, B.; Hensen, E. J. M. MKMCXX program; http://www.mkmcxx.nl.
(78) De Moor, B. A.; Reyniers, M.-F.; Marin, G. B. *Phys. Chem. Chem. Phys.* **2009**, *11*, 2939−2958.
(79) De Moor, B. A.; Ghysels, A.; Reyniers, M.-F.; Van Speybroeck, V.; Waroquier, M.; Marin, G. B. *J. Chem. Theory Comput.* **2011**, *7*, 1090−1101.
(80) van de Runstraat, A.; van Grondelle, J.; van Santen, R. A. *Ind. Eng. Chem. Res.* **1997**, *36*, 3116−3125.
(81) van Santen, R. A.; Niemantsverdriet, J. W. In *Chemical Kinetics and Catalysis*; Springer US: Boston, MA, 1995; p 153.
(82) Campbell, C. T.; Sellers, J. R. V. *J. Am. Chem. Soc.* **2012**, *134*, 18109−18115.

DOI: 10.1021/acscatal.7b02877
ACS Catal. 2017, 7, 8613−8627